Shear wave velocity structure beneath the Archaean granites around Hyderabad, inferred from receiver function analysis

VINOD K GAUR[1] and KEITH F PRIESTLEY[2]

[1] *Centre for Mathematical Modelling and Computer Simulation, NAL Belur Campus, Bangalore 560 037, India*
[2] *Department of Earth Sciences, Bullard Laboratories, University of Cambridge, UK*

Broadband receiver functions abstracted from teleseismic P waveforms recorded by a 3-component Streckeisen seismograph at Hyderabad, have been inverted to constrain the shear velocity structure of the underlying crust. Receiver functions obtained from the Hyderabad records of both shallow and intermediate focus earthquakes lying in different station-event azimuths, show a remarkable coherence in arrival times and shapes of the significant shear wave phases: *Ps*, *PpPs*, *PsPs/PpSs*, indicating horizontal stratification within the limits of resolution. This is also supported by the relatively small observed amplitudes of the tangential component receiver functions which are less than 10% of the corresponding radial component. Results of several hundred inversions of stacked receiver functions from closely clustered events (within 2°), show that the crust beneath the Hyderabad granites has a thickness of 36 ± 1 km, consisting of a 10 km thick top layer in which shear wave velocity is 3.54 ± 0.07 km/sec, underlain by a 26 ± 1 km thick lower crust in which the shear wave velocity varies uniformly with a small gradient of 0.02 km/sec/km. The shear wave velocity at its base is 4.1 ± 0.05 km/sec, just above the moho transition zone which is constrained to be less than 4 km thick, overlying a 4.74 ± 0.1 km/sec half space.

1. Introduction

Hyderabad (17.417°N, 78.55°E) is located on the Archaean granite terrane of the southern Indian craton. These granites have a Rb-Sr age of 2600 Ma, and are dominated by alkali feldspars (potassic) unlike the tonalitic (sodic) granites of the country further south in Karnataka (figure 1). The granitization process that created such a large volume of batholithic proportions potassium enriched rocks (Sarvothaman *et al* 1987), remains a mystery and although several studies (Rai *et al* 1996) have led to estimates of the gross crustal properties, there is little definitive evidence regarding the nature of their finer structure. The recent availability of 3-component broadband seismic records from the GEOSCOPE station at NGRI, Hyderabad (HYB) however, presented a new opportunity for investigating the fine scale structure beneath the area using the highly discriminating receiver function analysis.

Receiver functions are selectively abstracted horizontal components of the P-waveform ground motion, which represent only the P to S converted phase (*Ps*) and multiples that are sensitive to the shear velocity structure beneath the recording station. These locally-generated shear phases however are far too weak compared with the dominating P phases to be easily discernible on most seismograms. Whilst the use of teleseismic P waveforms that arrive at a distant station ($\Delta \geqslant 30$) with constant horizontal phase velocities approximating a plane wave, simplifies analysis, their steep angle of incidence at the base of the lithosphere causes the amplitude of converted shear phases to be small. These converted phases can be selectively isolated (Langston 1979) to constitute a receiver function for the crustal structure, by deconvolving the vertical component of the P waveform from the corresponding horizontal components of the first 30–40 sec of the ground motion record.

Keywords. Hyderabad; crustal structure; shear velocity; receiver function.

Proc. Indian Acad. Sci. (Earth Planet. Sci.), **106**, Nos 1 & 2, June 1997, pp. 1–08

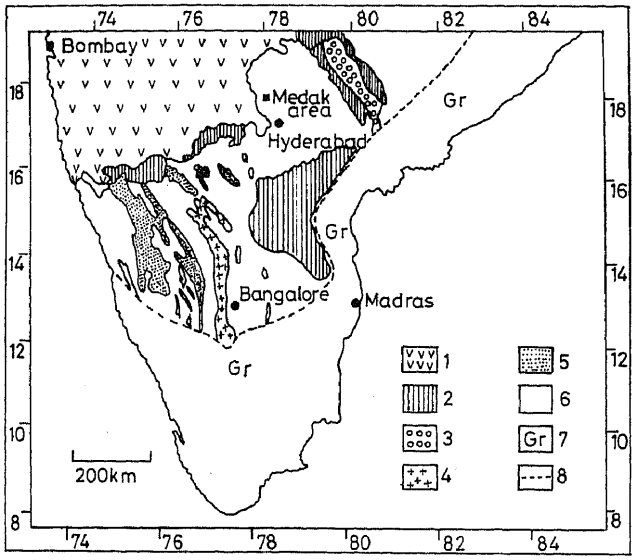

Figure 1. Simplified geological map of the southern Indian peninsular shield from Sarvothaman and Leelanandam (1987). (1) Deccan basalts; (2) Proterozoic formations; (3) Gondwanas; (4) Younger granites; (5) Dharwar Supergroup metasediments/volcanics; (6) Unclassified crystallines–granite-gneiss; (7) Granulite facies; (8) Granite-granulite boundary.

As shown by Ammon (1991), the receiver function thus obtained over a horizontally stratified earth, appears as a scaled version of the radial component of ground motion with the P multiples entirely eliminated. The deconvolution is accomplished by division in the Fourier transformed frequency domain and retransformation of the quotient back to the time domain. Let $V(t)$, $R(t)$ represent a ray description of the vertical and radial components of ground motion respectively and $V(W)$, $R(W)$ their Fourier domain counterparts. Then,

$$V(t) = \sum_k v_k S(t - t_k), \tag{1}$$

$$R(t) = \sum_k r_k S(t - t_k), \tag{2}$$

and the Fourier domain Receiver function

$$H(\omega) = \frac{R(\omega)}{V(\omega)}, \tag{3}$$

where, $S(t)$ is the source time function and t_k the instant of arrival of the kth ray, $k = 0$ representing the direct P phase.

In practice of course, one must band limit $V(\omega)$, $R(\omega)$ by using a Gaussian filter $F(\omega)$ of appropriate width, and also forestall instability deconvolution that may arise from division by spectral values of $V(\omega)$ that are either zero or very small. This can be done by constraining the lowest value of the denominator to remain above a practicable value set by a small parameter called the water level parameter (Clayton *et al* 1976).

Accordingly, one may rewrite (3) as

$$H(\omega) = \frac{R(\omega)V^*(\omega)F(\omega)}{\phi(\omega)}, \tag{4}$$

where, V^* is the complex conjugate of V, and

$$F(\omega) = f \exp\left(\frac{-\omega^2}{4a^2}\right) \tag{5}$$

is the Gaussian filter normalized to unit amplitude in the time domain by the factor f, and having a width a, and,

$$\phi(\omega) = \max[V(\omega)V^*(\omega),\ c \cdot \max\{V(\omega)V^*(\omega)\}], \tag{6}$$

$\phi(\omega)$ is set to the greater of the two quantities in parenthesis on the RHS of (6).

The corresponding time-domain receiver function $h(t)$ can then be shown (Ammon 1991) to be given by,

$$h(t) = \frac{r_0}{v_0}[\delta(t) + r_{sk}(t - t_k)],$$

where r_0 and v_0 are the vertical and horizontal amplitudes of the direct P phase and r_{sk}, those of the various converted shear wave phases.

It may be noted that a judicious choice of a and c is critical in determining the shape of the receiver function owing to their effects on the waveform spectra. In addition, the choice of c has to be a trade-off between the extent of such modification and stability of the deconvolution process. Options for such a choice can be delineated by abstracting receiver functions for a suite of a and c values and examining their signal quality, particularly of the self deconvolved vertical component.

The factor (r_0/v_0) scales the radial receiver function and therefore clearly depends on the epicentral distance as well as on the extent of contamination by scattered waves. In the original treatment of receiver function analysis, this quantity used to be normalized to unity, thereby obliterating the effect of varying epicentral distances (through the incidence angle of P waves), which is advantageous when stacking receiver functions from events covering a large geographical spread. This approach, however, forfeits valuable information implicit in this quantity, particularly that concerning the near surface velocity structure and estimates of contamination by scattering. Modern analysis of receiver functions, following (Ammon 1991), therefore retains the true amplitudes of the receiver functions and preserves the ratio (r_0/v_0) of the radial and vertical amplitudes of the P wave. In practice this is accomplished by deconvolving the vertical P wave from itself, which is seldom the expected delta function owing to spectrum modification by the water level and Gaussian parameters, and using its maximum amplitude to normalize the radial receiver function.

Before inverting receiver functions for velocity structure, it is desirable to reduce the effect of

random errors introduced by the computational process and earth noise. This can be achieved by stacking a number of receiver functions arising from closely spaced events (in our case within 2°). If records of an adequate number of such close events are not available and the signal to noise ratio of the receiver function unsatisfactory, recourse could be had to form composite receiver functions from a wider geographical spread of earthquakes, but in that case it would be necessary to suppress the range effect on individual receiver functions by normalizing the zero lag amplitude ratio (r_0/v_0) to unity.

It may be remarked here that whilst the tangential receiver function over a horizontal earth should ideally be zero, small amplitudes would generally appear in it owing to the presence of small levels of scattered energy in the seismograms. Significant finite amplitudes of tangential receiver functions therefore suggest departures from horizontal stratification and systematic variations of coherent phases, if present, can be used to infer the nature of inhomogeneity. The relative amplitudes of tangential and radial receiver functions are therefore an important guide in parameterizing the velocity structure to be inverted for.

Inversion of receiver functions to obtain the shear wave velocity structure is accomplished by parameterizing the latter in a manner so that the inverse problem is overdetermined i.e., the number n of data points d_j, is greater than the number m of unknown parameters of the velocity structure. For a layered earth model, this is normally defined as consisting of m layers each of constant thickness and uniform velocity m_k. The thickness of the layer is chosen to be such that it can be clearly resolved by the data phases being inverted. For example, in the case of predominantly 1.0 sec period shear waves having a wave length of over 3.5 km in the upper lithosphere, a layer thickness of 1–2 km should be quite satisfactory. When the earth model is so defined, determination of the velocity structure is reduced to the problem of estimating the unknown velocities in each of the m layers.

A usually satisfactory solution of an overdetermined inverse problem is given by the least squares solution which in principle, is unique. However, it may often produce unrealistically rapid velocity variations, owing to underdamping of the inversion process (as for example with unconstrained variance). Such situations can however, be circumvented by seeking a compromise solution which minimizes a chosen combination of the prediction error (data misfit) and model roughness (expressed for example by the second differences of model parameters).

Accordingly, we may express the basic statement of this inverse problem in a matrix form as follows:

$$\underset{n\times 1}{[\mathbf{d}]} = \underset{n\times m}{[\mathbf{F}]}\ \underset{m\times 1}{[\mathbf{m}]}, \tag{7}$$

where $[\mathbf{d}]$ is a vector of data points for n arguments, $\mathbf{m}$ the vector of velocities in different layers, and $\mathbf{F}$ is the functional that relates $\mathbf{m}$ to $\mathbf{d}$.

However, since (7) is nonlinear, we first seek the best solution $\mathbf{m}$ in the neighbourhood of an initial estimate $\mathbf{m}_0$ of the vector of layer velocities, which through some available means is considered closest to the true model, by linearizing it locally as follows:

$$\mathbf{Fm} = \mathbf{Fm}_0 + (\mathbf{D}_0, \delta\mathbf{m}) + 0|\delta\mathbf{m}|^2, \tag{8}$$

where, $\mathbf{m} = \mathbf{m}_0 + \delta\mathbf{m}$, and $(\mathbf{D}_0, \mathbf{m}_0)$ represent the inner product between $\mathbf{D}_0$ which is the partial derivative of $\mathbf{F}$ at $\mathbf{m}_0$, and the model correction vector $\delta\mathbf{m}$ being sought. Neglecting the smaller nonlinear terms $||\delta\mathbf{m}||$,

$$\mathbf{Fm} = \mathbf{Fm}_0 + (\mathbf{D}_0, \delta\mathbf{m}). \tag{9}$$

Since the inner product is linear i.e.,

$$(\mathbf{D}_0, \mathbf{m}) = (\mathbf{D}_0, \mathbf{m}_0) + (\mathbf{D}_0, \delta\mathbf{m}_0),$$

(9) can be written as:

$$[\mathbf{d} - \mathbf{Fm}_0 + (\mathbf{D}_0, \mathbf{m}_0)] = [\mathbf{D}_0, \mathbf{m}], \tag{10}$$

or,

$$\underline{\mathbf{d}} = \mathbf{Gm}, \tag{11}$$

where $\underline{\mathbf{d}}$ is the reconstituted data vector given by the quantities in the parenthesis on the LHS of (10) and $\mathbf{G}$ is the corresponding new functional that relates $\underline{\mathbf{d}}$ to $\mathbf{m}$. The relation (11) being linear, the solution of the smoothened (constrained) least squares inverse problem can now be written as (Menke 1989).

$$\underset{m\times 1}{[\mathbf{m}]} = [(\mathbf{G}'\mathbf{G} + \varepsilon^2\mathbf{H})^{-1}\mathbf{G}'][\underline{\mathbf{d}}],$$

where the prime denotes a transpose, ε the trade-off smoothness parameter and $\mathbf{H} = \mathbf{K}'\mathbf{K}$, $\mathbf{K}$ being the finite difference coefficient matrix

$$\begin{bmatrix} 1 & -2 & 1 & 0 & 0 & 0 & 0 & . \\ 0 & 1 & -2 & 1 & 0 & 0 & 0 & . \\ 0 & 0 & 1 & -2 & 1 & 0 & 0 & . \\ 0 & 0 & 0 & 1 & -2 & 1 & 0 & . \\ 0 & 0 & 0 & 0 & 1 & -2 & 1 & . \\ . & . & . & . & . & . & . & . \end{bmatrix}.$$

2. Data and analysis

3-Component broadband seismograms recorded at Hyderabad between May 1989 and March 1996 were obtained from the Geoscope data centre at Paris. Both radial and transverse receiver functions were generated from a large number of those for which broadband records were available, using different values of the Gaussian width a (5, 2.5, 1.0) and the

Table 1.

Year	Julian day	Latitude	Longitude	Depth km	Magnitude m_b
1990	150	45.841	26.668	89	6.7
1990	364	−5.097	150.967	179	6.6
1992	246	−6.046	112.138	625	5.9
1992	255	−6.087	26.651	11	6.7
1992	292	−6.279	130.214	119	5.8
1993	015	43.30	143.691	102	6.9
1994	104	−6.587	129.771	166	5.8
1994	194	−7.532	127.770	159	6.5
1994	271	−5.786	110.352	638	5.9
1994	319	−5.589	110.186	561	6.2
1995	235	18.856	145.218	595	6.3

water-level parameter c (0.0001, 0.001, 0.001, 0.01, 0.1). After a close scrutiny of the signal quality of these receiver functions, 11 of them (table 1), were selected for further analysis.

Figure 2, shows the receiver functions ($c = 0.001$, $a = 5.0$) obtained from 6 events, including both shallow and intermediate focus, from different azimuths. Their radial components show a remarkable coherence of phases. The time delays (3.9 ± 0.1 sec) of the *Ps* phase varies systematically with azimuth. This variation can be explained by two different velocity models: variations in the velocity structure of the mid to lower crust or variations in the Moho depth. However, possible variations, as will be shown later are estimated to be small, and coupled with the small relative amplitudes (< 10%) of the tangential receiver functions (figure 4), warrant the crust to be modelled as a predominantly one-dimensional structure on which small perturbations may be superposed.

Figure 3 shows the radial receiver functions ($c = 0.001$, $a = 2.5$) of 3 events clustered between 128° and 130°E and 6.35° and 7.5°S, as well as the stacked radial receiver function from these three events. Figure 4 compares this with another radial receiver function ($c = 0.001$, $a = 2.5$) stack composed of 3 events lying between 110° and 112°E and 5.6° and 6°S.

For inverting the stacked receiver functions, we adopted a starting reference model (dotted line in figure 5) based on some knowledge of the surface and average crustal velocities around Hyderabad (personal communication with Sri Nagesh and S S Rai). From this we generated a family of 20 new initial models (Ammon *et al* 1990) by adding to the reference model, a 2-component perturbation vector, with the purpose of obtaining a group of models which whilst being significantly different from each other would be expected to share some essential attributes of the parent model. The 2-component vector used to perturb the initial model consisted of a cubic perturbation vector scaled to a maximum velocity perturbation of 1.0 km/sec, and a random velocity change up to 20% of cubic perturbation.

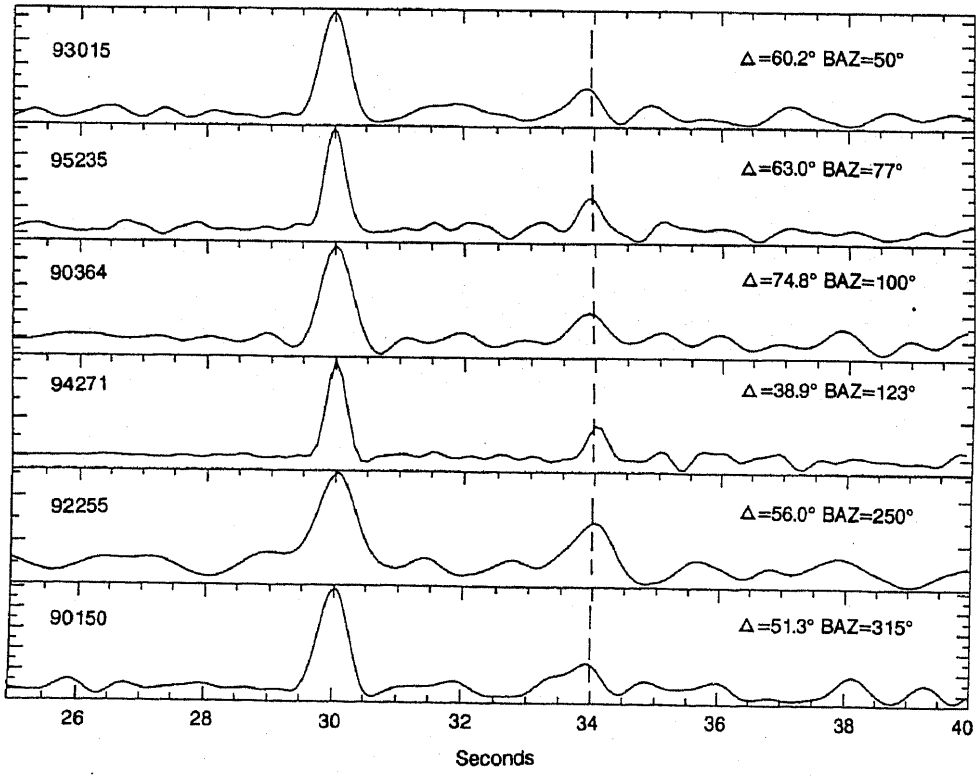

Figure 2. HYB single event radial receiver functions ($c = 0.001$, $a = 5.0$) plotted as a function of event azimuth. The higher frequency Gaussian was chosen in this case to better resolve time differences in the *Ps-P* delay. The distance and azimuth of the events from HYB are given to the right of each trace.

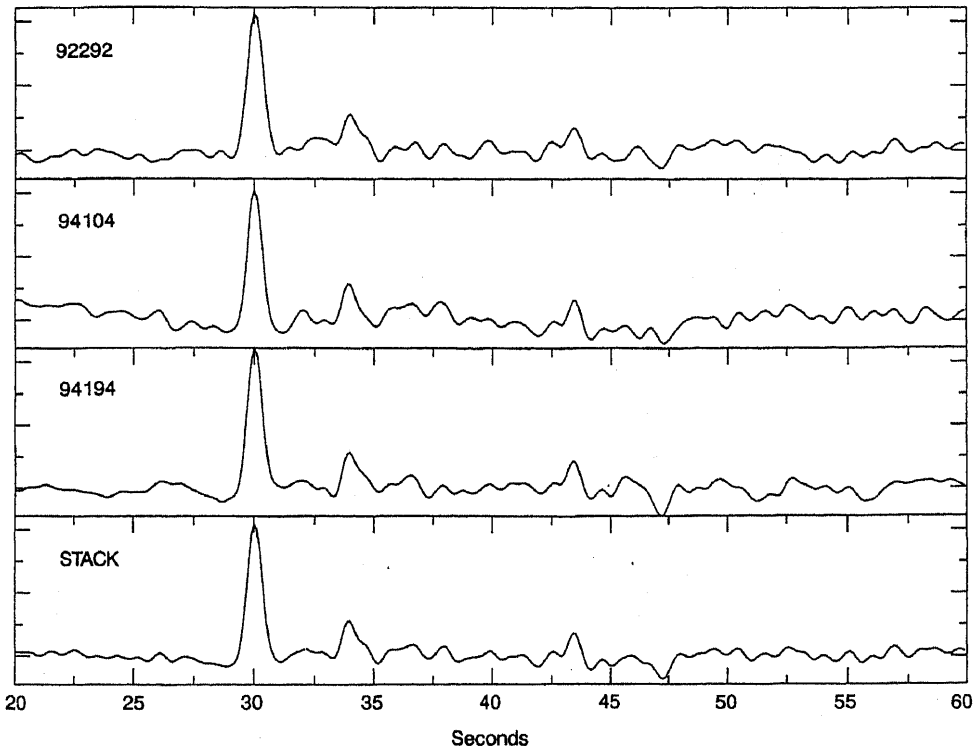

Figure 3. Three single event radial receiver functions ($c = 0.001$, $a = 2.5$) and the resulting radial stack for events lying between latitude 6.35 and 7.5° south and longitude 128 and 130° east.

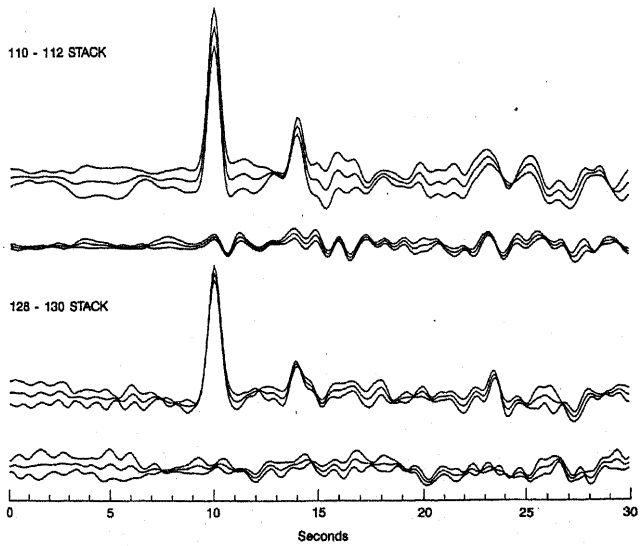

Figure 4. Comparison of two radial (the upper waveform in each) and tangential receiver function stacks used in the simultaneous inversion for the crustal structure beneath HYB. The upper pair of receiver functions are from three events lying between 5.6 and 6.0° south and longitude 110 and 112° east. The lower pair of receiver functions are from the events shown in figure 3. The mean and ± 1 standard deviation are shown.

Synthetic receiver functions were then computed using the same values of a and c (2.5, 0.001) selected earlier, and a P wave ray parameter (horizontal slowness) of 0.063 sec/km corresponding to a source approximately 60° away, to iterate the inversion process. Figure 5 shows the crustal models obtained after simultaneous inversion of the two stacked receiver functions shown in figure 4, for each of the initial models. Examination of several hundred such inversions, however, showed that the S wave velocity in the first 10 km was substantially uniform (3.48 ± 0.12 km/s).

This warranted investigation of a more constrained solution space in which shear wave velocity in the upper 10 km whilst free to excurse between the limits prescribed earlier, was held uniform. The result is shown in figure 6. The velocity range in the top layer that characterizes about 75% of all these models lay within a narrower limit $3.46 \leqslant V_s \leqslant 3.61$ kms.

Assuming that this range of top layer velocity shared by a majority of velocity solutions may approximate the real one more closely, we then imposed an additional constraint that the shear wave velocity in the top 10 km thick crustal layer should vary only within these limits.

The inverted velocity model of the Hyderabad crust subject to constraints suggested by these data is shown in figure 7.

3. Discussions and suggestions for future work

Receiver functions derived from the broadband seismograms recorded at Hyderabad and the inverted

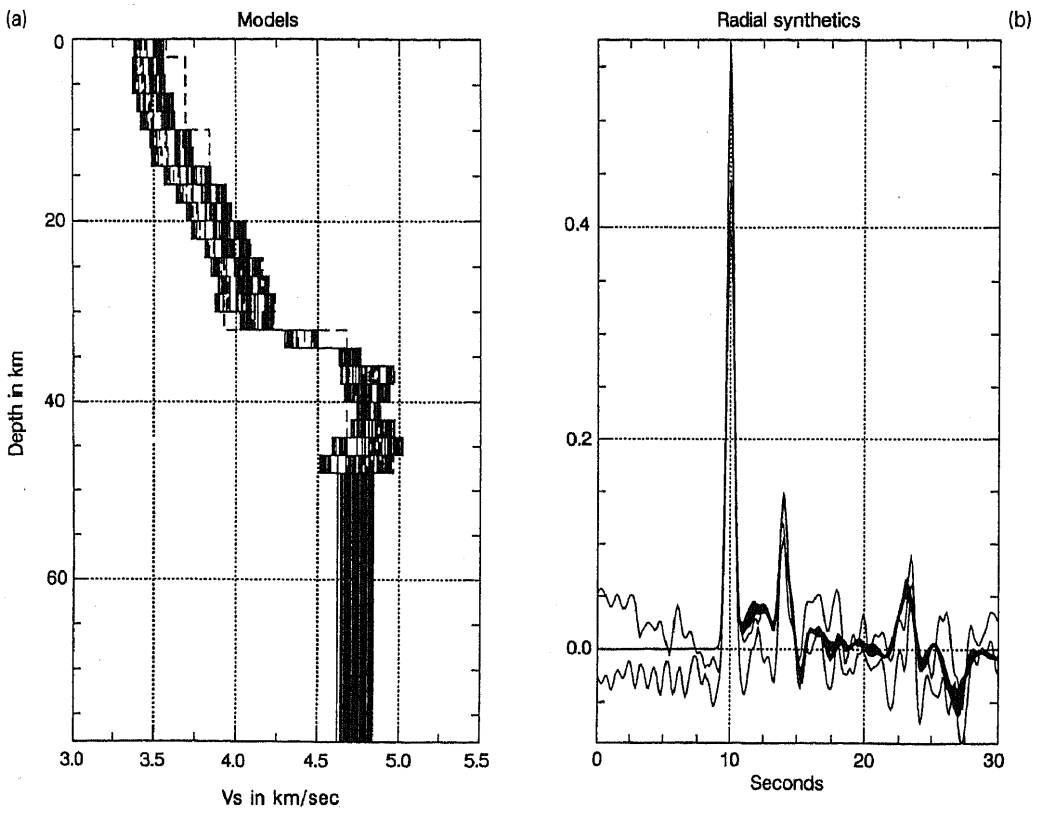

Figure 5. (**a**) Initial crustal models from the simultaneous inversion of the two radial receiver functions shown in figure 4. The dotted line denotes the initial starting model; (**b**) The fit of the resulting model synthetic radial receiver functions to the ± one standard deviation bounds.

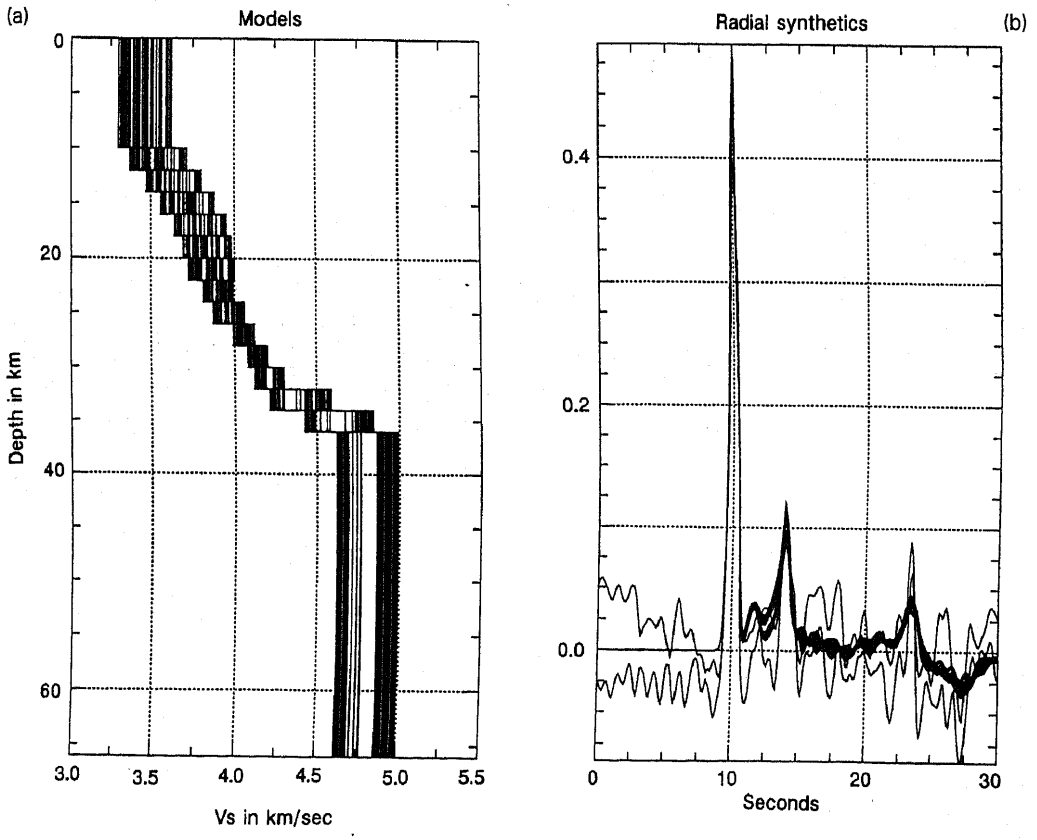

Figure 6. (**a**) Crustal models from the simultaneous inversion of the two radial receiver functions shown in figure 4, after constraining the surface layer to be 10 km thick; (**b**) The fit of the resulting model synthetic radial receiver functions to the ± one standard deviation bounds.

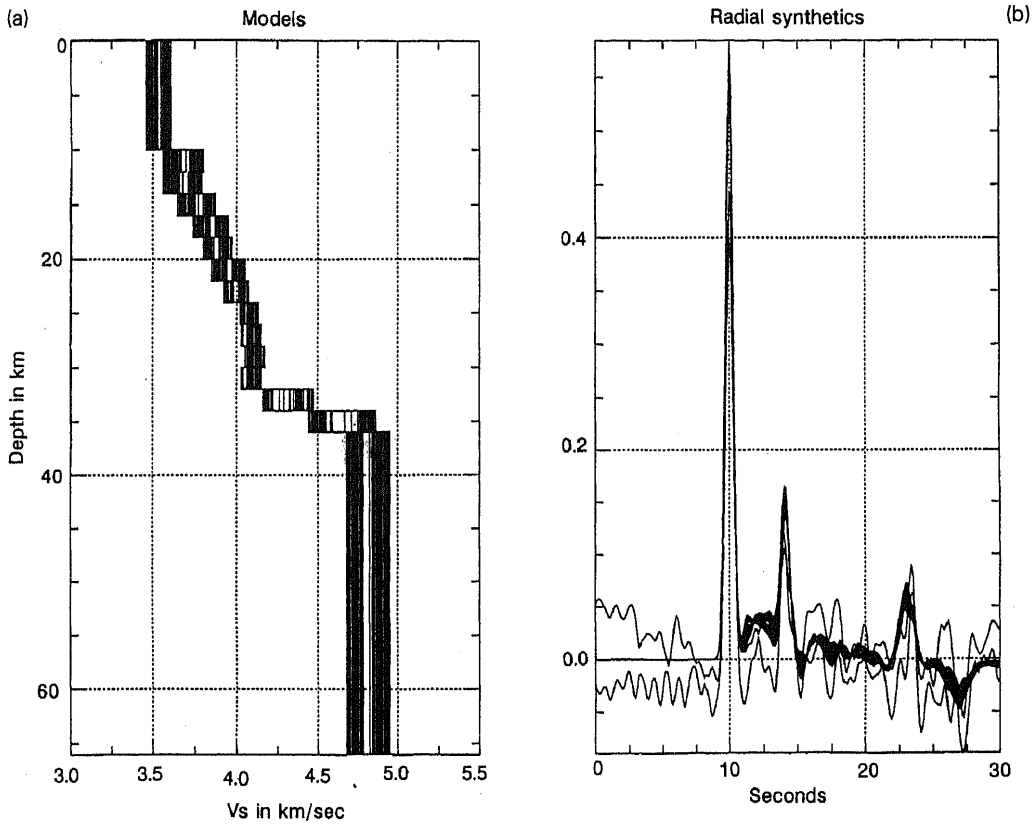

Figure 7. (**a**) Final crustal models from the simultaneous inversion of the two radial receiver functions shown in figure 4, after constraining the surface layer to be 10 km thick, and the shear wave velocity of this layer to lie in the range 3.46 to 3.61 km/sec; (**b**) The fit of the resulting model synthetic radial receiver functions to the ± one standard deviation bounds.

shear velocity structure reveal a number of significant features, and suggest some potentially illuminating approaches to future work.

Firstly, the radial receiver functions at Hyderabad are seen to be remarkably clean indicating that scattered energy in the seismograms is quite small, a fact also borne out by the small relative amplitudes of the transverse receiver functions. The latter observation also suggests that the velocity structure beneath Hyderabad is predominantly one-dimensional with possible second order perturbations. Secondly, the radial receiver functions show a high degree of coherence in the delay time intervals and shapes of the various converted S phases. In particular, the delay in the Ps phase (3.9 ± 0.1) shows a small but systematic variation with azimuth. This could have resulted from a systematic variation in the crustal velocity with azimuth or by variations in Moho depth. If the inhomogeneity is spread over the entire 36 km thick crust, it would correspond to about ± 0.10 km/s variation in the shear velocity, or to ± 0.14 km/sec if all this occurs in the lower 26 km of the crust. On the other hand, if the azimuthal variations in the delay of the Ps phase are caused by lateral variations in the Moho depth, the corresponding variations in the latter would be about ± 1.0 km.

Inverted velocity models show that the granite crust around Hyderabad has a more or less uniform top layer of 10 km thickness in which the shear velocity is 3.54 ± 0.07 km/sec, underlain by the lower crust of 26 ± 1 km thickness in which the velocity increases to about 4.1 ± 0.05 km/sec at its base, just above the Moho transition zone.

The Hyderabad crust thus appears to be largely homogeneous although the results of this analysis apply only to a small circular area of about 35 km radius, equal to the region of primary sensitivity of the Ps phase. The crustal structure further away from Hyderabad, however, is most likely quite different as suggested by radically different geological terranes (figure 1) on all sides of it: the Godavari rift and the eastern ghat granulites to the northeast and east, the Proterozoic Cudappah basin to the southeast, the tonalite granites, and the Dharwars and Deccan basalts to the south, southwest and west. Such a variegated geological setting of the Precambrian crust in the region must be the result of different crustal processes whose relict signatures most likely still preserved in the deep structure of the larger region around Hyderabad, hold illuminating clues to early crustal genesis and the nature of its resource and hazard environments. A logical follow up to this work would be to investigate this by deploying an array of

broadband seismographs covering the southern and eastern ghat granulites, the Cudappah and Gondwana basins, the Deccan volcanic province and the Dharwar craton and its enclaves of Proterozoic basins. Finally, because of the relatively transparent crust beneath HYB, it would be possible to construct a 3-dimensional velocity model of this cratonic region (for example, Owens *et al* 1984; Randall *et al* 1994).

Also, it would be highly desirable to extend the receiver function analysis of Hyderabad seismograms to deeper levels in the lithosphere and subjacent mantle which may be carried out by sampling a longer time series up to several hundred seconds (Gurrola *et al* 1995) in view of potentially significant clues that they may contain.

Acknowledgements

The authors thank Paul Saunders, R N Singh, S S Rai, D S Ramesh, Sri Nagesh, D Guptasarma and P S Moharir for elucidating various issues through discussions. V K G acknowledges the gracious assistance provided by the Royal Society, the CSIR and the Indian National Science Academy for travel and living support for a 3-week visit to the University of Cambridge where most of the computations were done.

References

Ammon C J, Randall G E and Zandt G 1990 On the non-uniqueness of receiver function inversions; *J. Geophys. Res.* **95** 15303–15318

Ammon C J 1991 The isolation of receiver effects from teleseismic *P* waveforms; *Bull. Seism. Soc. Am.* **6** 2504–10

Clayton R W and Wiggins R A 1976 Source shape estimation and deconvolution of teleseismic body waves; *Geophys. J. R. Astr. Soc.* **47** 151–177

Gurrolla H, Eli Baker G and Minister J B 1995 Simultaneous time-domain deconvolution with application to receiver function analysis; *Geophys. J. Int.* **120** 537–543

Langston C A 1979 Structure under Mount Rainier, Washington, inferred from teleseismic body waves; *J. Geophys. Res.* **84** 4749–62

Menke W 1989 Geophysical data analysis: Discrete inverse theory (Acad. Press Inc.)

Owens T J, Zandt G and Taylor S R 1984 Seismic evidence for an ancient rift beneath the cumberland plateau, Tennessee; *J. Geophys. Res.* **89** 7783–95

Randall G E and Owens T J 1994 Array analysis of the large-aperture array of the 1988–89 PASSCAL Basin and range passive source seismic experiment; *J. Geophys. Res.* **116** 618–36

Rai S S, Sarma P V S S R, Prakasam K S and Rao V K 1996 Seismic evidence for thick and underplated late Archaean crust of eastern Dharwar craton; *Proc. Indian Acad. Sci. (Earth Planet. Sci.)* **105** 431–439

Sarvothaman H and Leelanandam C 1987 Petrography and major oxide chemistry of the Archaean granitic rocks of the Medak area, Andhra Pradesh; *J. Geol. Soc. India* **30** 194–209

MS received 16 November 1996; revised 17 December 1996